REAL- AND COMPLEX-VARIABLE IMPLEMENTATIONS OF THE CONSISTENT BOUNDARY ELEMENT METHOD IN TWO-DIMENSIONAL ELASTICITY: A COMPARATIVE ASSESSMENT

NEY AUGUSTO DUMONT
Department of Civil and Environmental Engineering, Pontifical Catholic University of Rio de Janeiro, Brazil

ABSTRACT
The collocation boundary element method has recently been entirely revisited by the author. Arbitrary rigid-body displacements, as for elasticity, are naturally taken into account, and traction force parameters are always in balance independently of problem scale and mesh discretization. For generally curved boundaries, the correct definition of traction force interpolation functions enables the enunciation of a general convergence theorem, the introduction of patch and cut-out tests, and, not least, a considerable simplification of the numerical implementations. Simple code schemes for the 2D formulation are proposed exclusively in terms of Gauss–Legendre quadrature for arbitrarily high – actually only machine-precision dependent – computational accuracy of results independently of a problem's geometry and topology. On the other hand, the complex-variable formulation of the problem leads to more simplicity of implementation and numerical results that seem less liable to round-off errors. We propose in this contribution the comparative assessment of the real- and complex-variable formulations regarding coding efficiency, computational effort, error estimation, and numerical precision and accuracy of results for applications that are topologically highly challenging, with source-field distances in the subnanometer range.
Keywords: boundary elements, consistent formulation, machine-precision integration, complex-variable formulation.

1 INTRODUCTION

We have recently proposed the entire reformulation of the collocation boundary element method (CBEM), which keeps its essence, as obtainable from the application of Somigliana's identity, but introduces paramount features that go back to the initial consistency concerns related to the variationally, hybrid boundary element method [1], incorporates concepts related to the adequate treatment of quasi-singularities for 2D problems [2], [3], revisits the formulation in terms of spectral consistency assessments [4], [5] and ends up with the introduction of important code-implementation improvements [6]. All these developments have culminated in the comprehensive proposition of the CBEM [7], in general, with 2D developments laid down in Dumont [8], [9]. Although we have introduced in Dumont [2] and Dumont and Noronha [3] the paradigm-shifting concept of complex quasi-singularity poles (in terms of the boundary parametric variable ξ that may eventually assume values $\xi_s = a \pm ib$ related to a general source point s), all developments had been proposed in terms of Cartesian real variables (x, y), for 2D problems. Quite recently, we have envisaged that the complex-variable reformulation of Dumont [8], thus in terms of $z = x + iy$, may eventually lead to overall simplification of the implemented code and contribute to meliorate the unavoidable round-off-error issues that arise in applications to extremely challenging topologies [10].

This short contribution conveys the comparative assessment of the real-variable formulation of Dumont [8] and its complex-variable counterpart proposed in Dumont [10]. Owing to space restrictions we only address the evaluation of stress results at internal

WIT Transactions on Engineering Sciences, Vol 135, © 2023 WIT Press
www.witpress.com, ISSN 1743-3533 (on-line)
doi:10.2495/BE460061

points, which is actually the most critical issue one may face particularly when dealing with extremely small source-to-field distances. Interested readers are referred to the abundant details given in Dumont [8]–[10].

2 BASIC PROBLEM OUTLINE

Whether using real or complex variables, the basic system matrix to be solved in the frame of the CBEM has the format

$$\mathbf{H}(\mathbf{d}-\mathbf{d}^p)=\mathbf{G}(\mathbf{t}-\mathbf{t}^p)_{ad} \tag{1}$$

In this equation, $\mathbf{H}$ is the square, double-layer potential matrix of order $n_d=2n_n$, for 2D elasticity and the problem discretized with n_n nodal points, and $\mathbf{G}$ is the single-layer potential matrix with n_d rows and n_d+2n_e columns, as we code for n_e elements of any order o_e, in principle taking into account that the left and right tangents at a nodal point connecting two elements are different. As laid down in Dumont [5], [7], we are assuming just for the sake of elegant and compact formulation that some *particular* solution of interest is known – whether or not related to non-zero body forces – and may be approximately expressed as boundary nodal displacement $\mathbf{d}^p$ and traction $\mathbf{t}^p$ data. The problem's primary boundary displacement and traction parameters are $\mathbf{d}$ and $\mathbf{t}$, which are in part known and in part to be obtained in the frame of a general mixed-boundary formulation. As comprehensively assessed in Dumont [4], [7]–[9], we write for consistency that the traction $(\mathbf{t}-\mathbf{t}^p)_{ad}$ is *admissible*, in equilibrium with the applied domain forces: this follows the same mathematical/mechanical principle that, since for a finite domain rigid-body displacement amounts of $(\mathbf{d}-\mathbf{d}^p)$ cannot be transformed into forces, also non-equilibrated forces should not be transformed into displacements.

3 EVALUATION OF STRESS RESULTS AT INTERNAL POINTS

3.1 Real-variable formulation

We follow the notation given in Dumont [8] to represent stress results at an internal point s according to the expression given, for instance, in Brebbia et al. [11], although with some index transposition while always keeping in mind the traction-force interpolation given by eqn (20) of Dumont [7], for integration carried out along successive boundary segments of Γ in terms of the parametric variable $\xi\in[0,1]$:

$$\begin{aligned}\sigma_{is}=\sigma_{is}^p&+|J|_{(at\ \ell)}\int_\Gamma u^*_{is\ell}N^{o_e}_{(at\ \ell)}\,\mathrm{d}\xi\,(t_\ell-t^p_\ell)_{ad}\\&-\int_\Gamma p^*_{isn}N^{o_e}_{(at\ n)}|J|\,\mathrm{d}\xi\,(d_n-d^p_n)\end{aligned} \tag{2}$$

In this expression, σ_{is} is the symmetric stress tensor and

$$u^*_{is\ell}\equiv-\sigma^*_{is\ell}=\frac{(1-2\nu)(r_{,i}\delta_{s\ell}+r_{,s}\delta_{i\ell}-r_{,\ell}\delta_{is})+2r_{,\ell}r_{,i}r_{,s}}{4\pi(1-\nu)r} \tag{3}$$

$$\begin{aligned}p^*_{isn}=&\,G\frac{(1-2\nu)r_{,n}\delta_{si}+\nu(\delta_{ns}r_{,i}+\delta_{ni}r_{,s})-4r_{,i}r_{,s}r_{,n}}{\pi(1-\nu)r^2}\frac{\partial r}{\partial n}\\&+\frac{G}{2\pi(1-\nu)}\{2\nu\,(r_{,i}r_{,n}n_s+r_{,s}r_{,n}n_i)-(1-4\nu)\delta_{si}n_n\\&+(1-2\nu)(2r_{,i}r_{,s}n_n+\delta_{ni}n_s+\delta_{ns}n_i)\}\end{aligned} \tag{4}$$

In these equations, repeated indices mean summation and a comma (,) in the subscript means derivative with respect to the corresponding Cartesian direction 1 or 2, referring to x or y. The unit normal to the boundary is characterized by n and its Cartesian projections are also given. The Kronecker delta is given as δ_{si}, for instance. Boundary displacement and traction are approximated along successive segments by the scalars $N^{o_e}_{(at\ n)}(\xi)$ and $|J_{(at\ \ell)}|N^{o_e}_{(at\ \ell)}(\xi)/|J(\xi)|$, in terms of known *nodal* $(d_n - d^p_n)$ and *locus* $(t_\ell - t^p_\ell)_{ad}$ data – according to the important, corrected, formulation of the CBEM proposed in Dumont [5], [7]. The superscript o_e stands for the polynomial interpolation order, here implemented for linear, quadratic, cubic and quartic elements. Since repeated indices mean summation, we use $(at\ n)$ and $(at\ \ell)$ in eqn (2) to indicate that the shape functions refer to node n and locus ℓ [7]. The interpolation functions $N^{o_e}_{(at\ n)}$ and $N^{o_e}_{(at\ \ell)}$ have local support: the boundary integration along Γ prescinds the specific indication of sum over segments. The tractions are assumed to be *admissible*, that is, in balance with applied domain forces (whether void or not), which is the reason of the assigned subscript $(\ )_{ad}$ [4], [7]. Moreover, as proposed in Dumont [7], [8], we already take into account eventual *particular* or body-force solutions, characterized by the superscript $(\ )^p$, whenever this is mathematically feasible [7].

In the code implementation of Dumont [8], we express the stress tensor as a vector $\boldsymbol{\sigma} \equiv \langle \sigma_x \ \ \sigma_y \ \ \tau_{xy} \rangle^{\mathrm{T}}$, and $u^*_{is\ell}$ and p^*_{isn} as arrays

$$u^*_{is\ell} = \frac{1}{2\pi\,(1-\nu)} \left\{ \frac{0.5-\nu}{r^2} \begin{bmatrix} x & -y \\ -x & y \\ y & x \end{bmatrix} + \frac{1}{r^4} \begin{bmatrix} x^3 & x^2y \\ xy^2 & y^3 \\ x^2y & xy^2 \end{bmatrix} \right\} \tag{5}$$

$$p^*_{isn} = \frac{G}{2\pi(1-\nu)|J|} \left\{ \frac{1}{r^2} \begin{bmatrix} y' & -x' \\ y' & -x' \\ -x' & y' \end{bmatrix} + \frac{1}{r^4} \begin{bmatrix} 4x^2y' - 2xyx' & 2xyy' \\ -2xyx' & -4y^2x' + 2xyy' \\ 2xyy' & -2xyx' \end{bmatrix} - \frac{8(xy' - yx')}{r^6} \begin{bmatrix} x^3 & x^2y \\ xy^2 & y^3 \\ x^2y & xy^2 \end{bmatrix} \right\} \tag{6}$$

where, quoting [8], "$n_x = y'/|J|$ and $n_y = -x'/|J|$. In these expressions, the rows correspond to the elements of the stress vector defined above and the columns to the Cartesian directions represented by s. The subscripts ℓ and n are implicit as the reference to the field points related to $N^{o_e}_{(at\ \ell)}$ and $N^{o_e}_{(at\ n)}$ for the function multiplications and eventual integrations indicated by eqn (2). Moreover, the matrix components have been manipulated in order to make the quasi-singularity terms $1/r^2$, $1/r^4$ and $1/r^6$ explicit (they do not necessarily reflect the actual quasi-singularity powers), which is paramount for the subsequent developments."

3.2 Complex-variable formulation

It is proposed in Dumont [10] the complex-variable expression for stress results at internal points

$$\begin{Bmatrix} \sigma_x + \sigma_y \\ \sigma_y - \sigma_x + 2i\tau_{xy} \end{Bmatrix}_s = \begin{Bmatrix} \sigma^p_x + \sigma^p_y \\ \sigma^p_y - \sigma^p_x + 2i\tau^p_{xy} \end{Bmatrix}_s + \frac{|J|_{(at\ \ell)}}{4\pi(1-\nu)} \int_\Gamma N^{o_e}_\ell \begin{bmatrix} \frac{1}{z} & \frac{1}{\bar{z}} \\ -\frac{\bar{z}}{z^2} & -\frac{3-4\nu}{z} \end{bmatrix} \mathrm{d}\xi \begin{Bmatrix} (t-t^p)_{ad} \\ (\bar{t}-\bar{t}^p)_{ad} \end{Bmatrix}_\ell$$

$$-\frac{iG}{2\pi(1-\nu)}\int_{\Gamma} N_n^{o_e}\begin{bmatrix} \dfrac{z'}{z^2} & -\dfrac{\bar{z}'}{\bar{z}^2} \\ \dfrac{\bar{z}'}{z^2}-2\dfrac{\bar{z}z'}{z^3} & -\dfrac{z'}{z^2}\end{bmatrix} \mathrm{d}\xi \begin{Bmatrix} d-d^p \\ \bar{d}-\bar{d}^p \end{Bmatrix}_n \tag{7}$$

which is just a very compact way of writing eqn (2) – thus comprising all subsequent, auxiliary expressions. The displacement and traction parameters at *nodes* n and *loci* ℓ are complex values and their respective conjugate representations, as for displacements at a node n: $d = d_x + id_y$. The stress components are advantageously arranged as shown on the left, so that the cumbersome, real-variable arrays of the former section become the indicated simple expressions of the complex $z = x + iy$ and its conjugate. As developed in Dumont [10], we do not need to resort to the literature on complex-variable elasticity to arrive at the above equation, although the compact stress representation is certainly an inspiration from Muskhelishvili [12].

Besides its simplicity, there are some added advantages in using the latter expression. In fact, as shown in Dumont [10], we no longer need to distinguish between real and complex quasi-singularity poles, which simplifies the code implementation substantially. However, the most important advantage is that, as we see in the latter expression, the singularities we have to deal with are of the type $1/z$, $1/z^2$ and $1/z^3$ in terms of the complex pole $\xi_s = a + ib$, whereas in the former section, as given in the last paragraph, we may have quasi-singularities up to $1/r^6$ of the complex double-pole $\xi_s = a \pm ib$. Apart from that, most of the conceptual and code-implementation developments of Dumont [8] are used in Dumont [10].

The complete developments and code-implementation issues for 2D potential and elasticity problems are given in Dumont [8] and [10] in terms of real and complex variables, and are outlined above rather briefly for the most critical case of evaluating results at internal points. Numerical assessments are shown in the following for a simple problem that is made challenging on purpose, as well as for a second, actually extremely challenging, problem.

4 APPLICATION TO AN INFINITE PLATE WITH A HOLE

Fig. 1 shows on the left the geometric discretization of an infinite plate with a hole of unit radius. The solution for a uniform stress field $\sigma_{xx} = 1$, $\sigma_{yy} = \tau_{xy} = 0$ applied at infinity, according to Sadd [13], for instance, is compactly expressed in polar coordinates as

$$\begin{aligned}
\sigma_{rr} &= \frac{1}{2}\left(1-\frac{a^2}{r^2}\right)+\frac{1}{2}\left(1-4\frac{a^2}{r^2}+3\frac{a^4}{r^4}\right)(2\cos^2\theta-1) \\
\sigma_{\theta\theta} &= \frac{1}{2}\left(1+\frac{a^2}{r^2}\right)-\frac{1}{2}\left(1+3\frac{a^4}{r^4}\right)(2\cos^2\theta-1) \\
\tau_{r\theta} &= \left(-1-2\frac{a^2}{r^2}+3\frac{a^4}{r^4}\right)\sin\theta\cos\theta
\end{aligned} \tag{8}$$

The maximum stress value is $\sigma_{\max} = \sigma_{\theta\theta}(r = a, \theta = \pm\pi/2) = 3$, and we also obtain the highest normal stress in the vertical direction $\sigma_{\theta\theta}(r = a, \theta = 0) = -1$. For the sake of reference, we express on the right in Fig. 2 the analytical stress results σ_x, σ_y, τ_{xy} of eqn (8) at the 18 internal internal points of the open domain given on the left – and as detailed next – with the indicated lines just connecting points.

As indicated in the figure, we discretize the circular cavity with 10 quartic elements and 40 equally spaced, equidistant nodes from the center – not taking advantage of the double symmetry. The main source of errors in this simulation is related to the fact that the circular surface is modeled with quartic polynomial elements, with non-smooth transition between elements. In fact, we measure for nodes 1, 5, 9, 13, 17, 21, 25, 29, 33 and 37 the same lack of

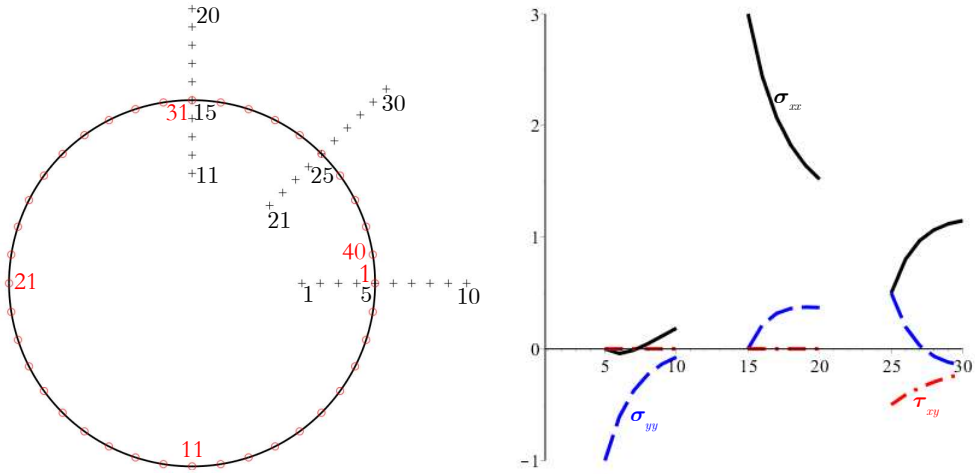

Figure 1: Infinite plate with a circular hole (left) modeled as 10 quartic elements; and analytical stress results evaluated at the indicated 18 internal points.

smoothness, with $(\theta^+ - \theta^-)/2\pi \approx 0.4999900076$, when it should be exactly $1/2$. Then, we should not expect in our numerical evaluations a relative accuracy error smaller than about 0.00001998. When evaluating results, points along a horizontal axis on the left in Fig. 1 that goes through nodes 21 and 1 should present the largest errors, as there is some angularity there. Tangents about nodes 11 and 31 are horizontal and we should expect the smallest errors measured along a vertical from there. Nodes 6, 16, 26 and 36, which are located at angles multiple of $\pi/4$ of inclination, do not have tangents inclined of exact multiples of $\pi/4$, since they are not middle nodes of the quartic elements. Such lacks of polar symmetry are intentional in order to have simulation errors introduced in our model. The figure also indicates three series of 10 points, each, at which stress results are to be evaluated. Points 1, 11 and 21 are $0.6 + 10^{-10}$ distant from the center, with interpolated points up to the respective points 10, 20 and 30, which are at a distance $1.5 + 10^{-10}$ from the center, in such a way that points $1 \ldots 4$, $11 \ldots 14$ and $21 \ldots 24$ are actually internal to the cavity, that is, external in relation to the open domain of interest. We intentionally set points 5, 15 and 25 inside the open domain and just 10^{-10} distant from the respective nodes 1, 31 and 36. Besides the geometry errors, we should expect some round-off errors related to these close points, as assessed next.

In both real- and complex-variable codes we use 8 Gauss–Legendre points per element, thus a total of 80 integration points for the whole problem. We also use 25 digits of precision in the Maple implementation (Maplesoft, a division of Waterloo Maple Inc., Waterloo, Ontario). This is by far more than necessary in the evaluation of matrices $\mathbf{G}$ and $\mathbf{H}$, to be used in eqn (1). In fact, in the precision evaluation $|\mathbf{HW} - \mathbf{W}|$, where $\mathbf{W}$ is a matrix with the three rigid-body displacements that the discretized circular hole may undergo, we obtain the global relative error of just 10^{-18} according to both codes. On the other hand, owing to the very small source-to-boundary distance 10^{-10}, as described above, severe round-off errors may be expected in the evaluation of stress results at points 5, 15 and 25.

Eqn (1) is solved for the displacement difference $(\mathbf{d} - \mathbf{d}^p)$ considering that $\mathbf{t} = \mathbf{0}$ and $\mathbf{t}^p$ corresponds to the proposed far stress field $(\sigma_{xx} = 1, \sigma_{yy} = \tau_{xy} = 0)$. Stress results

are subsequently evaluated according to eqns (2) and (7). Since the simulated problem corresponds to an applied constant stress field, the solution is considered exact for the proposed geometry, according to Theorem 1 of Dumont [7], within the adopted precision digits and numerical quadrature errors of the regular integrals involved. The distance threshold (relative distance from a source point to an element chord) is set equal to 2, in order to consider the source point sufficiently close as to require analytical corrections, according to Dumont [8]–[10]. This means that the numerical evaluations cannot be more precise than provided by the numerical quadrature – also considering the eventuality of round-off errors.

The graphs of Fig. 2 show the absolute errors – as compared with the analytical values for the circular cavity, according to eqn (8) – of the numerical stress results σ_{xx}, σ_{yy} and τ_{xy} at the 30 external and internal points described above. The dash, blue lines correspond to the real-variable evaluations of Section 3.1, and the solid, black lines correspond to the complex-variable evaluations of Section 3.2. Actual accuracy is assessed for results at the cavity points 1–4, 11–14 and 21–24, which should be zero regardless of boundary geometry approximation: the absolute errors – in general smaller than 10^{-6} – are attributable to the relatively low order of Gauss–Legendre quadrature for the large, high-order quartic elements, which may be improved by resorting to a higher quadrature or maybe by choosing a close/far threshold larger than 2. This is, however, not a useful measure, as there is already a larger geometry error in the piece-wise representation of the circular hole, as assessed above. And there is an information to draw from these assessments: our accuracy threshold is about 10^{-6}, which should be our precision threshold, as well. We see in Fig. 2 that the real- and complex-variable simulations deliver approximately the same accuracy of results, except that real-variable round-off-errors become excessively large at the critical, close point 5, while just reasonably large at points 15 and 25. On the other hand, the largest complex-variable, absolute errors of $(\sigma_{xx}, \sigma_{yy}, \tau_{xy})$ at point 5, close to an angularity and to be compared

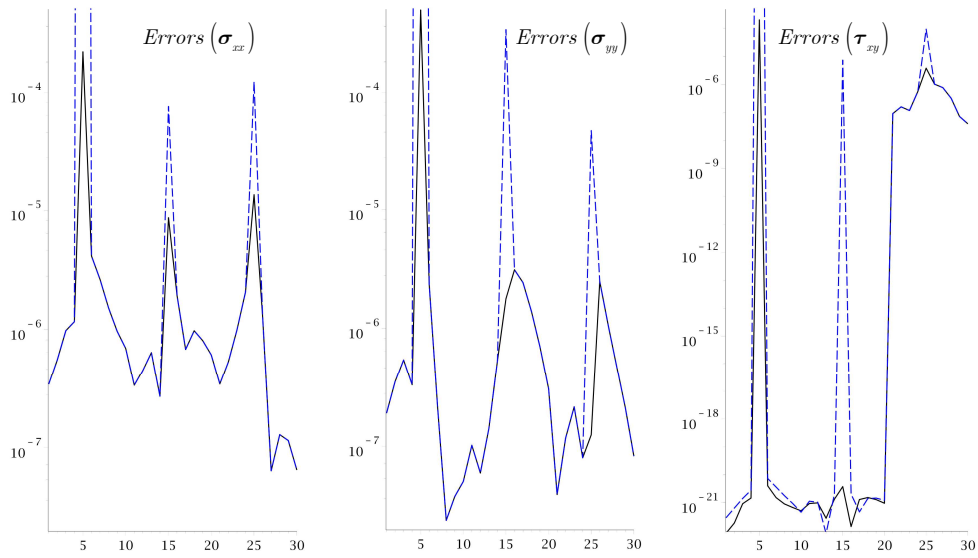

Figure 2: Absolute errors in the numerical evaluation of stress results σ_{xx}, σ_{yy}, τ_{xy} at 30 internal/external points for the infinite plate with a hole of Fig. 1, in terms of complex (solid, black lines) and real variables (dash, blue lines).

with $(0, -1, 0)$, are $(2.19 \times 10^{-4}, 4.92 \times 10^{-4}, 2.08 \times 10^{-4})$. At point 15, close to node 31 of a smooth surface and for stresses to be compared with $(3, 0, 0)$, these errors are $(6.81 \times 10^{-6}, 1.77 \times 10^{-6}, 3.78 \times 10^{-21})$. The errors at close point 25, for stresses to be compared with $(0.5, 0.5, -0.5)$, are $(1.35 \times 10^{-5}, 1.25 \times 10^{-7}, 3.87 \times 10^{-6})$.

5 APPLICATION TO A TOPOLOGICALLY EXTREMELY CHALLENGING PROBLEM

Fig. 3 represents a two-dimensional domain (about 25 units across) with some challenging topological features, to be subjected to a series of elastic fields, as described in Dumont [10], which is on the other hand a development of a simpler numerical model proposed in Dumont [9]. Readers are referred to these papers for the complete description of the problem. It is worth remarking that the cusp at node 1 has an internal angle of about 10^{-8} *rad*, the external angle at node 17 is of about 10^{-13} *rad*, and the strip of material between the cavity and the external boundary is only about 10^{-4} unities wide. This elastic body is subjected to two constant and a series of four linear, quadratic, cubic, quartic and quintic polynomial fields, thus a total of 22 fundamental solutions of the elastostatics problem for homogeneous, isotropic material with shear modulus $G = 80000$ and Poisson's ratio $\nu = 0.2$. The indicated crosses in Fig. 3 are a total of 41 – in part internal and in part external – points at which stress results are to be numerically evaluated for the applied stress fields. Some of these points are very close to the boundary, as described in Dumont [9], [10] and to be assessed next. Most important, we generate between internal point 30 and node 69, which are visually indistinguishable from each other in the figure, a series of 10 points that approach node 69 at geometrically decreasing distances, as indicated in the first row of Table 1, which is a reproduction from Dumont [10]. A similar series of 10 very close points to node 17 is also generated, with the distances indicated in the second row of this table. If we consider all

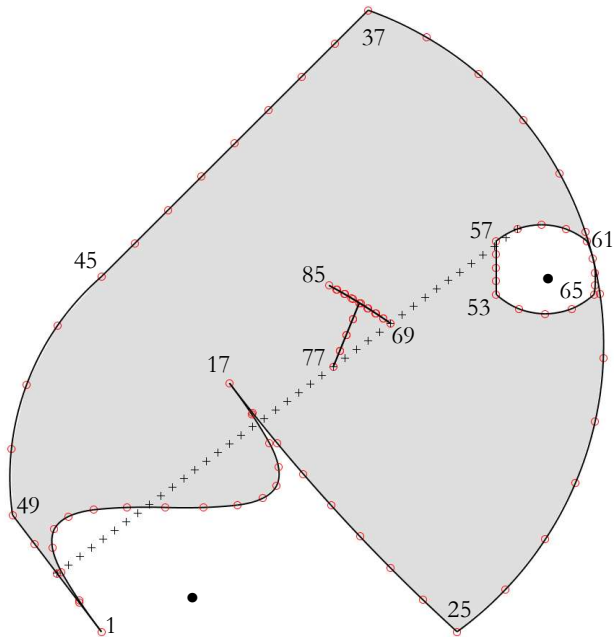

Figure 3: Two-dimensional figure with some challenging topological issues and to be subjected to a series of elastic fields, as reproduced from Dumont [10].

Table 1: Distances from very close points to their reference nodes in a mesh with 92 nodes, Fig. 3, as detailed in Dumont [10], from which this table is reproduced. The internal points 30 and P_0, with coordinates $\approx (16.27636, 17.35048)$ and $(7.19999, 14.00001)$, are close to nodes 69 and 17, respectively. The indicated distances refer to internal points numbered 42–51, on the left, and 52–61.

Internal $30 \to 69$	Internal $P_0 \to 17$
5.8947×10^{-17}	1.3120×10^{-18}
1.2378×10^{-15}	2.7552×10^{-17}
2.4816×10^{-14}	5.5235×10^{-16}
4.9639×10^{-13}	1.1048×10^{-14}
9.9280×10^{-12}	2.2097×10^{-13}
1.9856×10^{-10}	4.4194×10^{-12}
3.9712×10^{-9}	8.8388×10^{-11}
7.9424×10^{-8}	1.7677×10^{-9}
1.5884×10^{-6}	3.5355×10^{-8}
3.1769×10^{-5}	7.0710×10^{-7}

geometric data given in m, the smallest distances are actually about one thousandth of a typical proton size! As remarked in Dumont [10]: "This has absolutely no sense in terms of continuum mechanics but the mathematics must work nevertheless."

Dumont [9] deals with a similar problem to the one of Fig. 3 in terms of real variables, which is taken from Dumont [10] for a series of assessments of consistency and accuracy of eqn (1) as well as for displacement (not shown here) and stress results at internal points, using eqns (2) and (7), for different boundary element orders, numbers of Gauss–Legendre quadrature points, and precision digits. Papers [9] and [10] also have complete problem formulation and numerical assessments for potential problems.

We assess in the following the stress results for two numerical models considered in Dumont [10] – but not in Dumont [9] – in order to compare the proposed approaches directly. The first model is called 46_2_25_4 to characterize the use of $n_e = 46$ elements of order $o_e = 2$ (quadratic), for evaluations with 25 digits of precision and $n_g = 4$ Gauss–Legendre quadrature points per element. As for the real-variable formulation, there is a total of $n_e \times o_e = 92$ nodes, as indicated in Fig. 3, thus for the square matrix $\mathbf{H}$ of order $2 \times 92 = 184$ and the rectangular matrix $\mathbf{G}$ with $2 \times 92 = 184$ rows and $2 \times (92 + 46) = 276$ columns. The total number of Gauss–Legendre points is $46 \times 4 = 184$. It is worth repeating from Dumont [9] that a number of precision digits smaller than 20 would render the present problem inconsistent, as there would be interpenetration of the boundary faces adjacent to node 17.

A second model is called 23_4_50_8 to characterize the use of $n_e = 23$ elements of order $o_e = 4$ (quartic), for evaluations with 50 digits of precision and $n_g = 8$ Gauss–Legendre quadrature points per element. Then, all numbers given for the former model apply here, with the only – relevant – difference that 50 precision digits are used, and, of course, not neglecting that quartic elements enable better modeling than double the number of quadratic elements, as already assessed in Dumont [9] and [10].

The indicated matrix dimensions are actually not relevant for the only kind of numerical assessments we are showing, namely, the evaluation of stress results at internal/external points, according to eqns (2) and (7), for $d_n^p = 0$, $t_\ell^p = 0$, and the boundary displacement and traction parameters d_n and t_ℓ evaluated for the 22 polynomial fields of fundamental solutions.

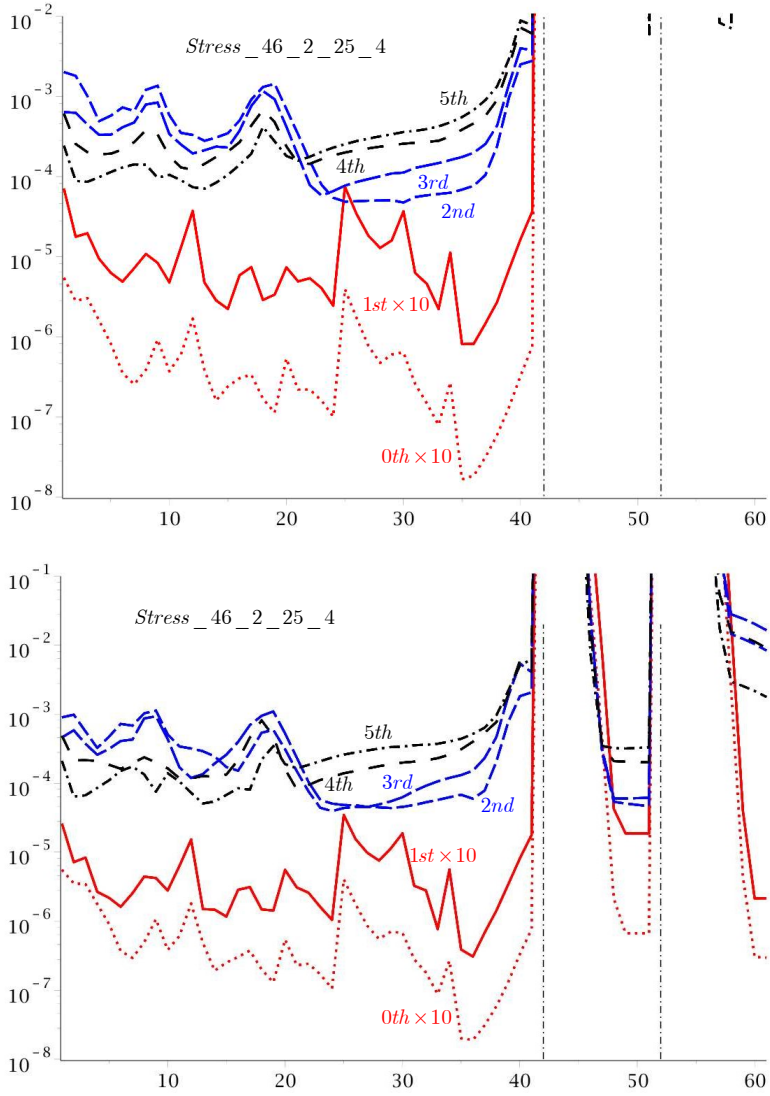

Figure 4: Errors in the evaluation of stress results along 61 internal/external points of Fig. 3, generated for six groups of elasticity test fields for the mesh configuration 46_2_25_4, in terms of real (top) and complex (bottom) variables. The bottom plot is a reproduction from Dumont [10].

Figs 4 and 5 show error results for stress evaluations at the 41 points marked as "+" in Fig. 3 (of which points 2 through 8 and 40 are actually external), as well as for the very close points numbered 42 through 61 referred to in Table 1, as given in the horizontal axes. Vertical dashdot lines are drawn to mark the closest points 42 and 52. Relative errors are given in the vertical log scale for groups of two constant displacements solutions (0th) and sets of four linear, quadratic, cubic, quartic and quintic solutions (1st, 2nd, 3rd, 4th and 5th, respectively). As given in Theorem 1 of Dumont [7] and pointed out in Dumont [9] and [10], the numerical

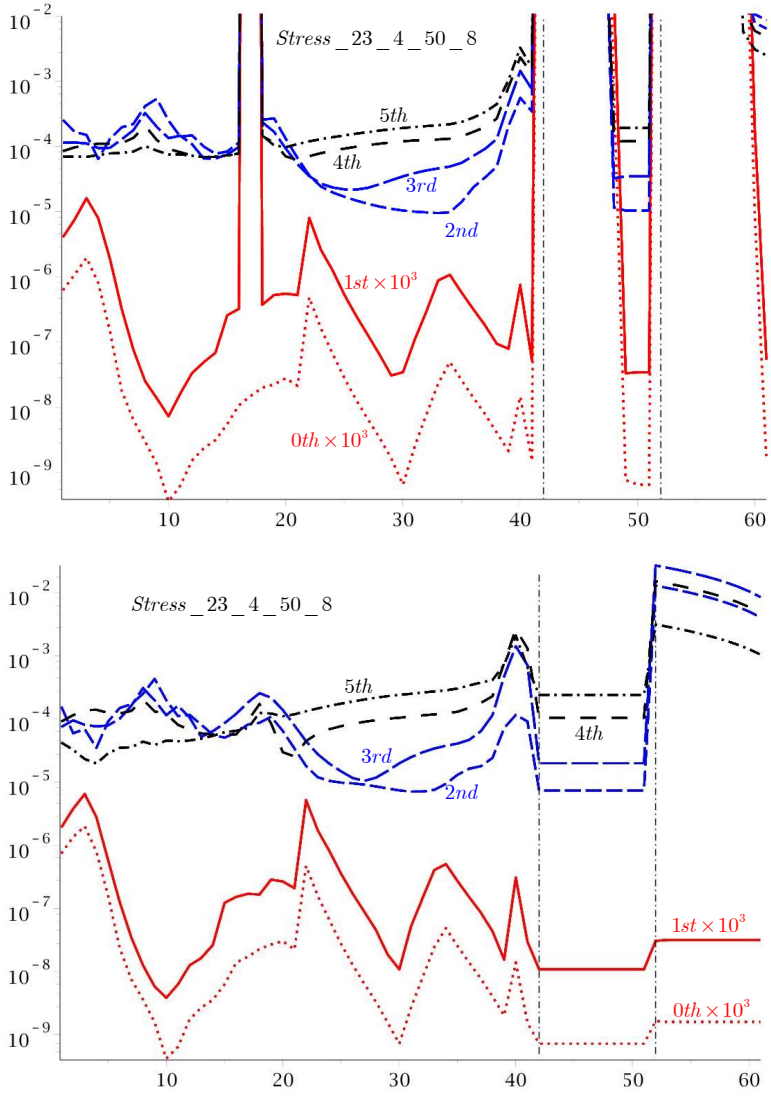

Figure 5: Errors in the evaluation of stress results along 61 internal/external points of Fig. 3, generated for six groups of elasticity test fields for the mesh configuration 23_4_50_8, in terms of real (top) and complex (bottom) variables. The bottom plot is a reproduction from Dumont [10].

evaluations for constant and linear solutions must correspond to analytical solutions of the problem – although within precision digits, number of Gauss–Legendre quadrature points and eventual round-off errors. Then, these solutions give the means of assessing the precision threshold of a numerical simulation. As indicated, the error results for constant and linear displacement fields are multiplied by powers of 10 in order to accommodate a better error resolution in the plots. In both figures the top graphs refer to evaluations in terms of real variables, to be compared with the bottom results in terms of a complex variable.

The real-variable and complex-variable results in each figure are comparable in terms of precision (results for 0th and 1st) and accuracy (for higher displacement fields), except for points that are too close to the boundary, as round-off errors take place and may become completely out of limits. We see in the top plot of Fig. 4 that real-variable results are reliable only for distances larger than about 10^{-7} (which, for unities in m, are smaller than a micrometer), whereas for the complex-variable evaluations we obtain reliable results for subnanometer distances about 10^{-10}. And that for "only" 25 digits of precision!

Fig. 5 presents – for in principle the same computational cost as for the previous evaluations – results that are several orders of magnitude more precise and one order of magnitude more accurate (a not lesser remark is that cost increases for the 50 digits of precision). This is related to the p-refinement from quadratic to quartic elements [9], [10]. Reliable results for the real-variable evaluations are achieved for distances that are orders of magnitude smaller than before, and this is to be credited to the large number of precision digits. On the other hand, results for internal points close to the (badly locally discretized) reentrance tend to be completely out of limits, as well as results for point 40, which is just outside the domain, tend to be more inaccurate, which is also related to the poor local mesh discretization. On the other hand, it is highly remarkable that the complex-variable evaluations shown on the bottom of Fig. 5 lead to reliable results up to the incredibly small distance of 10^{-18}. In fact, we see that the precision assessments for constant and linear displacement fields – and, then, Theorem 1 of Dumont [7] – holds just fine. Observe that here, too, the external point 40 is close to a locally coarse mesh, and consequently with relatively worse results. Moreover, observe that results at points 42 through 51 (piece-wise horizontal plots) are orders of magnitude more accurate than results at points 52 through 61 for the very simple reason that the corresponding local mesh – adjacent to node 17 – is very coarse.

6 CONCLUDING REMARKS

This brief outline and the simple, comparative numerical assessments show that the paradigm-shifting developments proposed in Dumont [7]–[9] may be still improved – in terms of code simplicity, cost and overall robustness – if we resort to a complex-variable formulation [10], as for 2D elasticity. The numerical illustrations refer once more to a highly important convergence Theorem 1 [7]; separately assess precision, accuracy, and liability to round-off errors; show that mesh refinement is required only to improve mechanical simulation, not for mathematical evaluations; and also show that we should not shun extreme cases of topological issues. A not lesser contribution is the illustration of the way three distinct geometric entities must be properly handled: *boundary nodes n* (for displacements), *boundary loci* ℓ (to which tractions are referred), and *domain points s*, at which we collocate the singular sources.

ACKNOWLEDGEMENT

This project was supported by the Brazilian federal agencies CAPES and CNPq, as well as by the state agency FAPERJ.

REFERENCES

[1] Dumont, N.A., The hybrid boundary element method: An alliance between mechanical consistency and simplicity. *Applied Mechanics Reviews*, **42**(11), pp. S54–S63, 1989.

[2] Dumont, N.A., On the efficient numerical evaluation of integrals with complex singularity poles. *Engineering Analysis with Boundary Elements*, **13**, pp. 155–168, 1994.

[3] Dumont, N.A. & Noronha, M., A simple, accurate scheme for the numerical evaluation of integrals with complex singularity poles. *Computational Mechanics*, **22**(1), pp. 42–49, 1998.
[4] Dumont, N.A., An assessment of the spectral properties of the matrix G used in the boundary element methods. *Computational Mechanics*, **22**(1), pp. 32–41, 1998.
[5] Dumont, N.A., The boundary element method revisited. *Boundary Elements and Other Mesh Reduction Methods XXXII*, ed. C.A. Brebbia, WIT Press: Southampton, pp. 227–238, 2010.
[6] Dumont, N.A., The collocation boundary element method revisited: Perfect code for 2D problems. *International Journal of Computational Methods and Experimental Measurements*, **6**(6), pp. 965–975, 2018.
[7] Dumont, N.A., The consistent boundary element method for potential and elasticity: Part I – Formulation and convergence theorem. *EABE – Engineering Analysis with Boundary Element Methods*, **149**, pp. 127–142, 2023.
[8] Dumont, N.A., The consistent boundary element method for potential and elasticity: Part II – Machine-precision numerical evaluations for 2D problems. *EABE – Engineering Analysis with Boundary Element Methods*, **149**, pp. 92–111, 2023.
[9] Dumont, N.A., The consistent boundary element method for potential and elasticity: Part III – Topologically challenging numerical assessments for 2D problems. *Engineering Analysis with Boundary Element Methods*, **151**, pp. 548–564, 2023.
[10] Dumont, N.A., Complex-variable, high-precision formulation of the consistent boundary element method for 2D potential and elasticity problems. *Engineering Analysis with Boundary Element Methods*, **152**, pp. 552–574, 2023.
[11] Brebbia, C.A., Telles, J.C.F. & Wrobel, L.C., *Boundary Element Techniques*, Springer-Verlag, 1984.
[12] Muskhelishvili, N.I., *Some Basic Problems of the Mathematical Theory of Elasticity*, Noordhoff International Publishing: Leyden, 1957.
[13] Sadd, M.H., *Elasticity, Theory, Applications, and Numerics*, Elsevier, 2005.